Homogeneous Nucleation of [dmim$^+$][Cl$^-$] from its Supercooled Liquid Phase: A Molecular Simulation Study

Xiaoxia He, Yan Shen, Francisco R. Hung and Erik E. Santiso

Abstract We have used molecular simulations to study the homogeneous nucleation of the ionic liquid [dmim$^+$][Cl$^-$] from its bulk supercooled liquid at 340 K. Our combination of methods include the string method in collective variables (Maragliano et al., J. Chem. Phys. 125:024106, 2006), Markovian milestoning with Voronoi tessellations (Maragliano et al J Chem Theory Comput 5:2589, 2009), and order parameters for molecular crystals (Santiso and Trout J Chem Phys 134:064109, 2011). The minimum free energy path, the approximate size of the critical nucleus, the free energy barrier and the rates involved in the homogeneous nucleation process were determined from our simulations. Our results suggest that the subcooled liquid (58 K of supercooling) has to overcome a free energy barrier of $\sim$85 kcal/mol, and has to form a critical nucleus of size $\sim$3.4 nm; this nucleus then grows to form the monoclinic crystal phase. A nucleation rate of 6.6×10^{10} cm^{-3} s^{-1} was determined from our calculations, which agrees with values observed in experiments and simulations of homogeneous nucleation of subcooled water.

Keywords Homogeneous nucleation · Ionic liquid · Molecular dynamics

X. He · Y. Shen · F.R. Hung (✉)
Cain Department of Chemical Engineering, Louisiana State University,
Baton Rouge, LA 70803, USA
e-mail: frhung@lsu.edu

F.R. Hung
Center for Computation & Technology, Louisiana State University, Baton Rouge,
LA 70803, USA

E.E. Santiso
Department of Chemical and Biomolecular Engineering, North Carolina State University,
Raleigh, NC 27695, USA

R.Q. Snurr et al. (eds.), *Foundations of Molecular Modeling and Simulation*,
Molecular Modeling and Simulation, DOI 10.1007/978-981-10-1128-3_7

1 Introduction

Room-temperature ionic liquids (ILs) have attracted significant attention as designer solvents, electrolytes, and other applications mostly involving liquid phases of the ILs. Very recently, Warner et al. [1–7] developed IL-based nanomaterials (dubbed GUMBOS, for Group of Uniform Materials Based on Organic Salts) where these compounds are in the solid state. These IL-based materials hold enormous promise, as they have the highly tunable properties of ILs [8, 9] and can be prepared via simple procedures [1–7], possibly impacting fields as diverse as optoelectronics, photovoltaics, separations, analytical chemistry and biomedicine. 1D-nanomaterials such as nanorods and nanowires were also synthesized [6] by introducing the ILs inside hard templates with cylindrical nanopores, e.g., multi-walled carbon nanotubes and anodic alumina membranes; shape anisotropy can lead to further variations in interesting properties of these nanomaterials (fluorescence, magnetic). On the other hand, ILs are also immobilized in nanoporous solids (carbon nanotubes, silica, cellulose, polymers, etc.) during the synthesis of ionogels [10]. These hybrid materials have potential applications in lithium batteries, fuel cells and solar cells, and in catalysis and biocatalysis, drug delivery and optical sensing devices [10]. A rational design of IL-based nanomaterials and ionogels require a fundamental understanding of the solidification, as well as the nucleation and growth of crystals of ILs in contact with surfaces and inside nanopores.

As a starting point for our studies in this area, here we focus on modeling the homogeneous nucleation of a simple IL, 1,3-dimethylimidazolium chloride, or [dmim$^+$][Cl$^-$], from its supercooled liquid phase in the bulk. This IL has been extensively studied in previous simulation reports [11–19]. However, nucleation is an extremely challenging problem [20–27], mainly because the initial stages of nucleation typically involve a few molecules or atoms, which makes it difficult to design experiments to study nucleation at the molecular level. Molecular dynamics (MD) simulations of nucleation are also very challenging, as nucleation is a rare event. Previous studies of homogeneous nucleation of systems of particles (hard-sphere, Lennard-Jones, etc.) [28–37] water [38–46] and other substances (e.g., NaCl, silicon, benzene, n-octane, urea, copper, aluminum, etc.) [47–58] using rare event methods have provided important insights on these phenomena in those systems. However, these methods might have limitations when studying the nucleation of ILs, which can have very slow dynamics and therefore the transition paths might take a prohibitively long time to commit to any of the stable states. Here we have combined the string method in collective variables (SMCV) [59] with Markovian Milestoning with Voronoi tessellations [60–62] to study the homogeneous nucleation of [dmim$^+$][Cl$^-$]. This combination of methods has been used before to study conformational changes in biomolecules [59, 61, 63, 64]. In the SMCV, a string of replicas connecting the liquid with the crystal phase evolves guided by the negative gradient of the free energy with respect to some collective variables (or order parameters, OPs, characterizing the transition), until they converge into a minimum free energy path (MFEP). This path represents the region

where the transition has the maximum probability to take place. This converged string is then used as input to our second method, Markovian milestoning with Voronoi tessellations, which yields the free energy along the path, as well as the mean first passage times (MFPTs) in the transition studied. In association with these methods we have used the OPs for molecular crystals recently developed by Santiso and Trout [65]. These OPs can distinguish between different crystal polymorphs and liquid phases, and detect crystal ordering in nm-size regions. For example, if our system would crystallize into two solid polymorphs, one could use our methods to determine the minimum free energy paths connecting the supercooled liquid with the different polymorphs, and comparison of the free energies of the polymorphs would provide insights about their thermodynamic stability.

We note here that we have used the same methods and OPs in previous studies of the homogeneous nucleation of benzene [66] and the same IL studied here, [dmim$^+$][Cl$^-$] [67]. In the latter report we used a system consisting of 1372 ion pairs, and interpreted our results using calculations based on classical nucleation theory, which also helped us address possible finite-size effects in this system. Our interpretations were corroborated by SMCV results obtained using a larger system containing 2268 ion pairs [67]. Here in this paper we present a complete account and discussion of our results obtained for this larger system, using both the SMCV and Markovian milestoning with Voronoi tessellations, which completes the work we have presented before [67]. Nucleation could be studied using alternative approaches such as transition path sampling/aimless shooting, and metadynamics (see, e.g. [54, 55]). However, for very complex systems such as ILs, which have slow dynamics, the transition paths might take a long time to commit to any of the stable states, and trajectories could recross the top of the barrier multiple times [54], which could make sampling extremely challenging. Furthermore, and in order to avoid finite-size effects, here we had to consider a relatively large system size (2268 ion pairs), which required us to use a total of 180 OPs. Such a system would be extremely challenging to study using metadynamics (systems previously studied with this method were significantly smaller and had a considerably lower number of collective variables, see, e.g. [55, 68]). The rest of the paper is structured as follows. In the next section, we provide details of our systems and methods (OPs used, SMCV and Markovian milestoning with Voronoi tessellations). Section 3 contains our main results and discussion, and our main findings are summarized in Sect. 4.

2 Simulation Details

2.1 Models

The monoclinic crystal structure of [dmim$^+$][Cl$^-$] was obtained from the Cambridge Crystallographic Data Centre [69, 70]. The classical, non-polarizable, all-atom force field developed by Lopes et al. [71–75] was used to model the IL, mainly because it

can reproduce the experimental crystal structure of [dmim$^+$][Cl$^-$] [71] (here the cations and anions have integer charges). Furthermore, the density of the liquid phase and the melting point as determined from simulations using this model were found to be in good agreement with experimental values [76]. Our system contained 2268 ion pairs, which can form a monoclinic crystal of characteristic dimensions 8.3 nm $\times$ 5.3 nm $\times$ 9.7 nm. All MD simulations were performed using a modified version of the NAMD software [77] that included implementations of the OPs, the SMCV and Markovian milestoning with Voronoi tessellations (see below) in C++ libraries. All the simulations were performed in the NPT ensemble with $P = 1$ bar and $T = 340$ K (a supercooling of 58 K). When selecting the temperature (and thus the degree of supercooling) in our systems, we considered the following aspects that would impact the computational costs of our simulations. Higher temperatures (i.e., smaller supercoolings) would result in an increase in the size of the critical nucleus. In this situation one could obtain a critical nucleus that might be larger than the dimensions of the simulation box, and run into finite-size issues; therefore a larger simulation box would be needed, which would increase computational costs. Reducing the temperature (i.e., having a larger supercooling) would reduce the size of the critical nucleus; however, if the temperature is too low, the dynamics of the ions would slow down and thus very long simulations would be needed. We have found that, for our system, 58 K of supercooling provides a system with reasonable dynamics, and allowed us to use a simulation box of reasonable size (so that the critical nucleus formed does not percolate through any of the dimensions of the box). A Langevin thermostat with a damping coefficient of 25 ps^{-1} was used to control the temperature, and the Nosé-Hoover Langevin piston with a damping time of 50 fs was used as the barostat. Periodic boundary conditions were applied in all directions. Lennard-Jones and electrostatic interactions were cutoff at 10 and 12 Å; particle mesh Ewald (PME) [78] was used to handle the latter type of interactions. Hydrogen bond lengths were constrained with the LINCS algorithm, and a time step of 0.5 fs was used in our simulation runs [79]. Additional details of our model systems can be found elsewhere [67].

2.2 Order Parameters (OPs)

The OPs developed by Santiso and Trout [65] are extracted from a generalized pair distribution function. All OPs used in this study were based on [dmim$^+$]; no particular OPs were defined for [Cl$^-$]. In Fig. 1 two ion pairs are shown, where the absolute orientation of each cation is given by the vectors q_1 and q_2, which are normal to the imidazolium ring of each cation. The distance OP provides quantification for the various center of mass (COM) distances between the cations. The bond orientation OP measures the orientation of bonds joining the center-of-mass of the cations, while the relative orientation OP measures the orientation of one cation with respect to another one [65, 67]. All the OPs are defined per cation and per peak

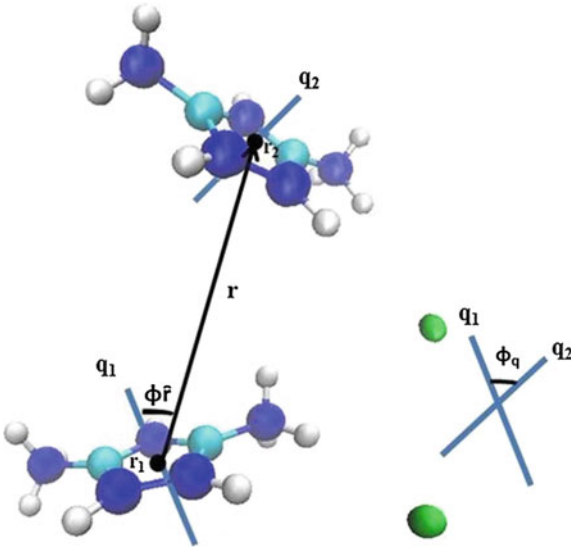

Fig. 1 Variables used in the construction of OPs. The vector normal to the plane of the imidazolium ring of [dmim$^+$] gives the absolute orientation of each of the two cations. The distance OP is based on r, which joins the center of mass (COM) of the two cations. The angle formed by the vectors r and q_1 is used for the bond orientation $\phi_{\hat{r}}$, whereas the angle formed by the vectors q_1 and q_2 is used for the relative orientation ϕ_q

in the pair distribution function, which leads to an extremely large number of OPs. To reduce the total number of OPs, we first sum over peaks in the pair distribution function, and then calculate local averages over the cations present in a given subcell of the simulation box, according to the following equation [65]:

$$\theta_C = \frac{1}{N_C} \sum_{i \in C} \sum_{\alpha} \varphi_{i,\alpha} \tag{1}$$

where N_C is the number of cations in subcell C, the index i denotes the ith cation, the index α runs over peaks of the pair distribution function, and $\varphi_{i,\alpha}$ represents any of the per-molecule and per-peak OP (i.e., distance, bond orientation or relative orientation). Therefore, each subcell has a corresponding OP. Additional details are presented elsewhere [65].

In our system, the simulation box was divided into 6 × 5 × 6 subcells, giving a total of 180 OPs of each type (distance, bond orientation and relative orientation). In Fig. 2 we present the number frequency of distance, bond orientation and relative orientation OPs for the liquid and crystal phases of [dmim$^+$][Cl$^-$] at 340 K. The frequency is averaged over 400 configurations (as obtained from short, 0.4 ns MD simulation of the liquid and solid phases in the NPT ensemble). These results indicate that any of the OPs can serve as a good metric to distinguish between crystal and liquid phases, even in nm-sized regions. Here we chose to work with the bond orientation OPs, although we also monitored the distance and the relative orientation OPs.

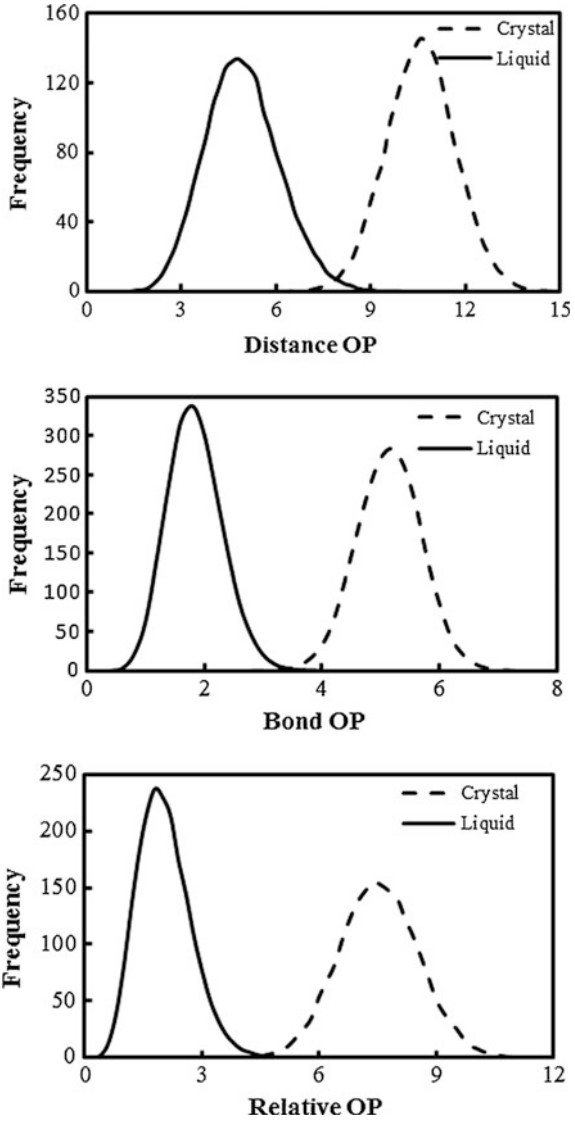

Fig. 2 The number frequency of distance, bond orientation and relative orientation OPs for liquid and solid IL, as obtained from 400 liquid-like and 400 crystal-like configurations of the IL. The distance, bond orientation and relative orientation OPs have units of $Å^{-1}$, which corresponds to the units of σ_α (see, e.g., Eqs. 11, 15, 21–22 in Ref. [65]; we used similar OPs here)

2.3 String Method in Collective Variables (SMCV)

The SMCV [59, 63] was used to sketch a MFEP for the homogeneous nucleation of $[dmim^+][Cl^-]$ from its subcooled liquid. Here we used the following procedure:

1. An initial string consisting of 32 replicas was prepared by collecting a number of intermediate states from the simulated melting of a crystal of the IL at 800 K.

Each replica i in this string contains 180 OPs (denoted by q_i) that characterize its local structure.

2. At every step of the SMCV method:

   2.1. An extended Hamiltonian is established for each replica, by including a set of harmonic springs that keep each replica's OPs close to their 'target' values. Using this extended Hamiltonian, we run short (0.2 ns) MD simulations in the NPT ensemble for each image, in order to determine the mean force $\nabla_q F(q_i)$ and metric tensor $M(q_i)$ required to maintain each image close to the target OP values (here the mean force is the negative gradient of the free energy with respect to the OPs)

   2.2. The new target OPs are estimated by taking a forward Euler step on the string evolution equation:

$$q_i^* = q_i - \Delta\tau M(q_i)\nabla_q F(q_i) \tag{2}$$

   where $\Delta\tau$ is the time step in the SMCV, and q_i^* denotes the target OPs for the ith image for the next SMCV step.

   2.3. Reparameterize by interpolating a curve through the new target OP values q_i^*, and recompute new target OP values q_i^* so that consecutive replicas are at constant arclength from each other. This step prevents the replicas from clustering near the stable states.

3. Step 2.1–2.3 above are repeated until the potential of mean force (PMF) converges; here the PMF is the line integral of the restraint force along the path in the multi-dimensional OP space

Additional details about the SMCV and its implementation are presented elsewhere [59, 63, 66, 67].

2.4 Markovian Milestoning with Voronoi Tessellations

The MFEP computed from the SMCV is an n-dimensional function (where n is equal to the 180 OPs), determined by effectively restraining 180 degrees of freedom as the replicas in the SMCV evolve following the negative gradient of the free energy with respect to the OPs. The MFEP thus only represents a single pathway in the transition tube. However, this tube can be mapped into a single free energy curve as a function of a reaction coordinate, by using the converged string from the SMCV as input to simulations using Markovian milestoning with Voronoi tessellations [60–63]. This procedure can also yield information about the rate of nucleation. In this method, we associate a cell in OP space to each replica from the converged SMCV string, forming a tessellation in the OP space. By construction [61, 63], the edges of the tessellations are approximate isocommittor surfaces, and thus are used as milestones in our procedure. We then perform MD simulations

where each replica is forced to remain within its own cell by using soft walls (planar half-pseudoharmonic restraints) [61]. In these simulations we monitor the number of collisions each trajectory does with the milestones (edges of the Voronoi tessellation). At steady state, if $N_{n,m}$ represents the number of collisions that the MD trajectory in cell B_n experiences with the boundary of cell B_m during the simulation time t_n, the rate of escape from tessellation cell B_n to cell B_m can be estimated as:

$$v_{n,m} = \frac{N_{n,m}}{t_n} \tag{3}$$

The probability π_n of finding the system in cell B_n can then be calculated from the following equations:

$$\sum_{\substack{n=1 \\ n\neq m}}^{N} \pi_n v_{n,m} = \sum_{\substack{n=1 \\ n\neq m}}^{N} \pi_m v_{m,n} \tag{4}$$

$$\sum_{n=1}^{N} \pi_n = 1 \tag{5}$$

The free energy curve F_n can be calculated as a function of cell n as follows:

$$F_n = -k_B T \ln \pi_n \tag{6}$$

In turn, the MFPTs can be also computed from the Voronoi milestoning procedure using the following equations:

$$\sum_{b\neq b^*} k_{a,b}\, t_{b,b^*} = -1, \quad a \neq b^* \tag{7}$$

$$k_{a,b} = \frac{\sum_{n=0}^{N} \pi_n N_{a,b}^n \Big/ t_n}{\sum_{n=0}^{N} \pi_n t_a^n \Big/ t_n} \tag{8}$$

where t_{b,b^*} is the MFPT to milestone b^* from other milestones in the system (where $b \neq b^*$). $k_{a,b}$ is the rate of instantaneous transition from milestone a to milestone b; $N_{a,b}^n$ is the total number of transitions from milestone a to milestone b during the simulation confined to cell B_n, and t_a^n is total time during which a was the most recent milestone visited by the system. We used the arbitrary precision floating-point library implemented in the Sage software [80] to solve the equations above, as the values of $k_{a,b}$ could have variations of up to 6 orders of magnitude. Additional details of these simulations are provided elsewhere [61, 63, 66, 67].

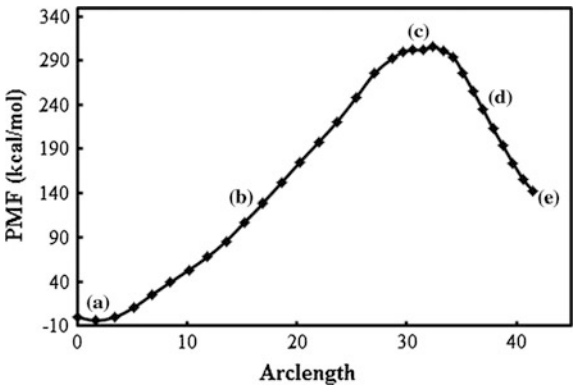

Fig. 3 The PMF associated with the MFEP for homogeneous nucleation of a crystal phase of [dmim$^+$][Cl$^-$] from its supercooled liquid phase at 340 K and 1 bar. The *left* and *right sides of the curve* correspond to crystal and liquid states. Simulation snapshots of states labeled here are shown in Fig. 4

3 Results and Discussion

3.1 Determination of the MFEP from the SMCV

The converged PMF (see Sect. 2.3) as determined from our simulations with the SMCV is presented in Fig. 3; here the arclength (of the bond orientation OPs, in this case) represents the distance along the multidimensional nucleation path. A difference of about 141 kcal/mol is observed between the crystal phase and the supercooled liquid phase at about 58 K of supercooling, with a PMF barrier of about 163 kcal/mol between the supercooled liquid and the state at the top of the PMF profile.

In Fig. 4 we show *x*–*y* side views of representative simulation snapshots of several relevant states along the MFEP mapped in Fig. 3. As we move left from the supercooled liquid (state e) at the right of the PMF curve shown in Fig. 3, the cations and anions start to rearrange (state d) until we reach the top of the barrier (state c), where the ions form a critical nucleus exhibiting crystal-like order. If we arbitrarily define the cations with OPs > 3.5 (Fig. 2) as crystalline, those cations form a cluster in the replica at the top of the PMF curve (the critical nucleus) which has an average size of $\sim$3.4 nm at this degree of supercooling. A similar procedure was used for the configuration at the top of the free energy curve (Fig. 6) determined from our Voronoi milestoning simulations (see below), giving a similar average size for the critical nucleus. Moving further left (and now downhill) along the MFEP mapped in Fig. 3, the crystal-like region grows (state b) until the system crystallizes completely (state a).

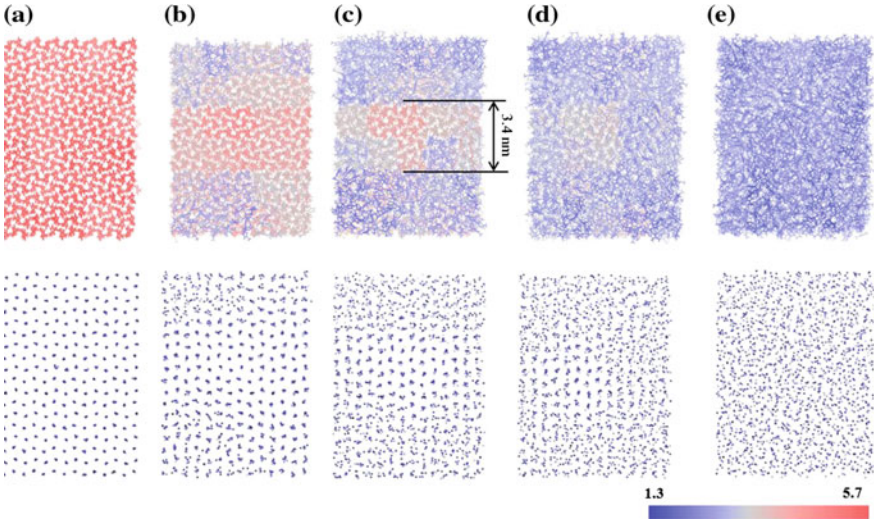

Fig. 4 *x–y* side views of simulation snapshots of states labeled along the MFEP shown in Fig. 3. The cations (*top row*) are *color-coded* according to the value of their bond orientation OPs (*red* crystal-like, *blue* liquid-like). The anions are shown on *bottom row* and are *not color-coded*

3.2 *Free Energy and MFPTs from Markovian Milestoning with Voronoi Tessellations*

The 32 replicas from the converged SMCV string were used as the starting point for our series of simulations with Markovian milestoning. Here we had to interpolate additional replicas (to reach a total of 74) as to ensure collection of enough statistics for the numerical solution of Eqs. (3–8). As direct analysis of the data is difficult due to the 180-dimensionality of the OP space, we used principal component analysis to determine the subspace of the OP space that contains most of the variance along the solidification path. In Fig. 5 we show the projections onto the first two principal components of the initial configurations (converged SMCV string, black dots), as well as some representative configurations (different colors) observed throughout our Markovian milestoning simulations. The results shown in Fig. 5 suggest that the images mainly remain within their own cells, although they occasionally wander into neighboring cells for a brief period; this is a consequence of using soft walls [61] to maintain each MD trajectory within its own cell. One important challenge is to properly distribute the images along the MFEP, in order to accumulate good statistics for the numerical solution of Eqs. (3–8). At the same time, we strived to not place too many images in MFEP regions with high curvature; this way, replicas mostly visit adjacent cells when they leave their own cells, and we avoid transitions between non-adjacent cells as much as possible (as discussed before [63], replicas visiting cells of non-adjacent neighbors can affect the accuracy in the calculations of the free energy and the MFPTs).

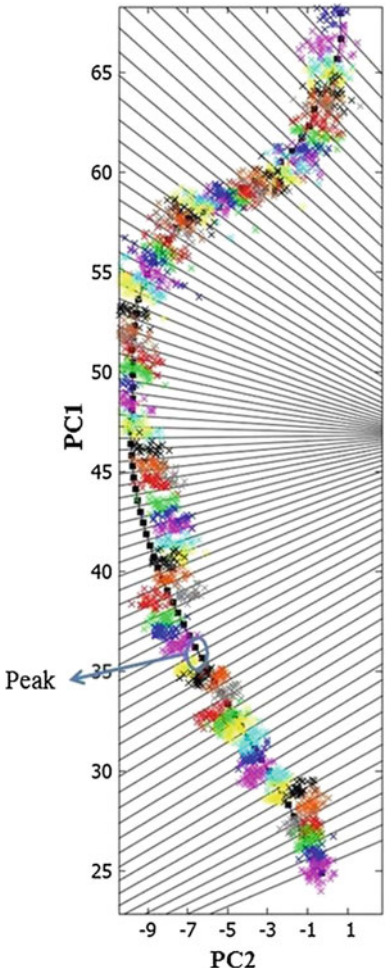

Fig. 5 Voronoi tessellation of the MFEP as projected onto the first two principal components PC1 and PC2 in OP space. The *black dots* represent the initial configurations (converged SMCV string plus interpolation of additional replicas) used in the Markovian milestoning simulations. Projections of representative configurations obtained from the milestoning procedure are also shown using *different colors*. The region corresponding to the peak of the PMF and free energy curves (Figs. 4 and 6) is labeled

In Fig. 6 we show the free energy along the MFEP as a function of the Voronoi cell number, as determined from the Voronoi milestoning simulations. These results indicate that the difference in free energy between the crystal and liquid phases of [dmim$^+$][Cl$^-$] at 58 K of supercooling is about 50 kcal/mol, and the free energy barrier between the liquid and the configuration at the top of the curve is about 85 kcal/mol. These free energy differences are comparable to those determined for water [41] and urea [55] in recent simulation studies of homogeneous nucleation. The free energy curve (Fig. 6) and the PMF curve (Fig. 3) are qualitatively similar (the snapshots of configurations obtained from the Markovian milestoning simulation procedure look very similar to those obtained from the SMCV and shown in Fig. 4); however the differences in free energies between relevant states are smaller than the corresponding differences in PMF. This observation is expected, as in the

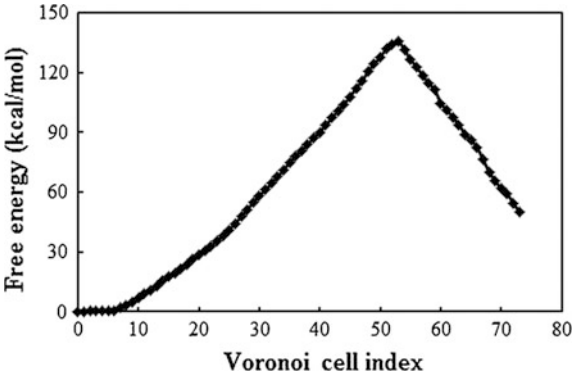

Fig. 6 Free energy involved in the homogeneous nucleation of [$dmim^+$][Cl^-] from its supercooled liquid phase at 340 K and 1 bar, as obtained from the milestoning procedure. The *left* and *right sides of the curve* correspond to crystal and liquid states

SMCV more entropy is removed as we are effectively restraining 180 degrees of freedom (replicas evolve guided by the negative gradient of free energy in order parameter space). In contrast, in the Markovian milestoning simulations less entropy is removed from the system, as by construction a trajectory restrained to remain in its Voronoi cell is equal to the equivalent sections of a conventional (unbiased) MD trajectory that is passing through the same cell [61].

In Fig. 7 we show the MFPTs to reach the configurations at the peak of the free energy curve (Fig. 6). Here we only considered fluxes between adjacent cells (fluxes between non-adjacent cells represent about 13 % of the total number of fluxes in our milestoning simulations). If we consider all fluxes (i.e. between nearest and non-nearest neighboring images), we determined that the difference in MFPTs with respect to those shown in Fig. 7 is only of about 8 %. These results suggest that the contribution of non-adjacent isocommittor surfaces to the kinetics of the nucleation process can be ignored (for a detailed discussion, see Appendix B in the study of Ovchinnikov et al. [63]). The results shown in Fig. 7 suggest that the MFPTs to the configurations at the peak of the free energy curve of Fig. 6 are approximately constant for milestones $B_{i+1} \cap B_i$ with $i = 72, 71, \ldots, 53$. From the data shown in Fig. 7, we calculated a simulated nucleation rate of 6.6×10^{10} cm^{-3} s^{-1} for our system, which is at a supercooling of 58 K. Unfortunately no experimental data is available for our system; however, our computed rate is in

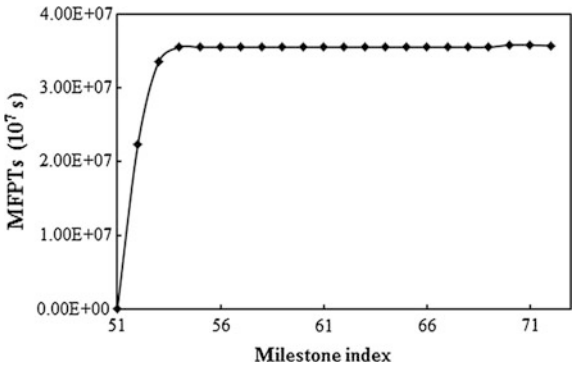

Fig. 7 Mean first passage times (MFPTs) from the milestone $B_{i+1} \cap B_i$ for $i = 72, 71, \ldots 52$ to the milestones at the shoulder of the free energy curve, $B_{52} \cap B_{51}$

reasonable agreement with experimental and simulation values for the homogeneous nucleation of ice, which are on the order of 10^{10} cm^{-3} s^{-1} [41, 81, 82] at a supercooling of about 40 K.

4 Conclusions

The homogeneous nucleation of the IL [dmim$^+$][Cl$^-$] from its bulk subcooled liquid phase (58 K of supercooling) was studied using molecular simulation. The SMCV [59, 63] combined with OPs [65] for molecular crystals was used to have a string of replicas map a MFEP connecting the supercooled liquid with the monoclinic crystal phase. The converged SMCV string was then used to initiate simulations using Markovian milestoning with Voronoi tessellations [61, 63]. These methods yield information about the free energy barrier, the size of the critical nucleus and the rate of nucleation. Our results indicate that the supercooled liquid has to overcome a free energy barrier of $\sim$85 kcal/mol to form a critical nucleus of size $\sim$3.4 nm. A simulated homogeneous nucleation rate of 6.6×10^{10} cm^{-3} s^{-1} was determined from our calculations. The values of the free energy barrier and the rate of nucleation are in reasonable agreement with experimental and simulation values obtained for the homogeneous nucleation of water and urea. Current work in our group is focused on the study of nucleation of ILs near surfaces and inside pores.

Acknowledgments We are grateful to Isiah Warner and his group (Chemistry, LSU) for helpful discussions. This work was partially supported by the National Science Foundation (CAREER Award CBET-1253075, and EPSCoR Cooperative Agreement EPS-1003897), and by the Louisiana Board of Regents. High-performance computational resources for this research were provided by High Performance Computing at Louisiana State University (http://www.hpc.lsu.edu) and by the Louisiana Optical Network Initiative (http://www.loni.org).

References

1. Tesfai, A., El-Zahab, B., Bwambok, D.K., Baker, G.A., Fakayode, S.O., Lowry, M., Warner, I.M.: Controllable formation of ionic liquid micro- and nanoparticles via a melt-emulsion-quench approach. Nano Lett. **8**, 897–901 (2008)
2. Tesfai, A., El-Zahab, B., Kelley, A.T., Li, M., Garno, J.C., Baker, G.A., Warner, I.M.: Magnetic and nonmagnetic nanoparticles from a group of uniform materials based on organic salts. ACS Nano **3**, 3244–3250 (2009)
3. Bwambok, D.K., El-Zahab, B., Challa, S.K., Li, M., Chandler, L., Baker, G.A., Warner, I.M.: Near-Infrared fluorescent NanoGUMBOS for biomedical imaging. ACS Nano **3**, 3854–3860 (2009)
4. Das, S., Bwambok, D., El-Zahab, B., Monk, J., de Rooy, S.L., Challa, S., Li, M., Hung, F.R., Baker, G.A., Warner, I.M.: Nontemplated approach to tuning the spectral properties of cyanine-based fluorescent nanogumbos. Langmuir **26**, 12867–12876 (2010)

5. Dumke, J.C., El-Zahab, B., Challa, S., Das, S., Chandler, L., Tolocka, M., Hayes, D.J., Warner, I.M.: Lanthanide-based luminescent NanoGUMBOS. Langmuir **26**, 15599–15603 (2010)
6. de Rooy, S.L., El-Zahab, B., Li, M., Das, S., Broering, E., Chandler, L., Warner, I.M.: Fluorescent one-dimensional nanostructures from a group of uniform materials based on organic salts. Chem. Commun. **47**, 8916–8918 (2011)
7. Warner, I.M., El-Zahab, B., Siraj, N.: Perspectives on moving ionic liquid chemistry into the solid phase. Anal. Chem. **86**, 7184–7191 (2014)
8. Thomas, W.P.W.: Ionic Liquids in Synthesis. Wilet-VCH, Weinheim (2008)
9. Plechkova, N.V., Seddon, K.R.: Applications of ionic liquids in the chemical industry. Chem. Soc. Rev. **37**, 123–150 (2008)
10. Le Bideau, J., Viau, L., Vioux, A.: Ionogels, ionic liquid based hybrid materials. Chem. Soc. Rev. **40**, 907–925 (2011)
11. Sha, M., Wu, G., Fang, H., Zhu, G., Liu, Y.: Liquid-to-solid phase transition of a 1,3-dimethylimidazolium chloride ionic liquid monolayer confined between graphite walls. J. Phys. Chem. C **112**, 18584–18587 (2008)
12. Sha, M., Wu, G., Liu, Y., Tang, Z., Fang, H.: Drastic phase transition in ionic liquid Dmim CI confined between graphite walls: new phase formation. J. Phys. Chem. C **113**, 4618–4622 (2009)
13. Pinilla, C., Del Popolo, M.G., Kohanoff, J., Lynden-Bell, R.M.: Polarization relaxation in an ionic liquid confined between electrified walls. J. Phys. Chem. B **111**, 4877–4884 (2007)
14. Pinilla, C., Del Popolo, M.G., Lynden-Bell, R.M., Kohanoff, J.: Structure and dynamics of a confined ionic liquid. topics of relevance to dye-sensitized solar cells. J. Phys. Chem. B **109**, 17922–17927 (2005)
15. Youngs, T.G.A., Hardacre, C.: Application of static charge transfer within an ionic-liquid force field and its effect on structure and dynamics. ChemPhysChem **9**, 1548–1558 (2008)
16. Hanke, C.G., Atamas, N.A., Lynden-Bell, R.M.: Solvation of small molecules in imidazolium ionic liquids: a simulation study. Green Chem. **4**, 107–111 (2002)
17. Del Popolo, M.G., Lynden-Bell, R.M., Kohanoff, J.: Ab initio molecular dynamics simulation of a room temperature ionic liquid. J. Phys. Chem. B **109**, 5895–5902 (2005)
18. Buhl, M., Chaumont, A., Schurhammer, R., Wipff, G.: Ab initio molecular dynamics of liquid 1,3-dimethylimidazolium chloride. J. Phys. Chem. B **109**, 18591–18599 (2005)
19. Monk, J., Singh, R., Hung, F.R.: Effects of Pore size and pore loading on the properties of ionic liquids confined inside nanoporous CMK-3 carbon materials. J. Phys. Chem. C **115**, 3034–3042 (2011)
20. Debenedetti, P.G.: Metastable Liquids: Concepts and Principles. Princeton University Press, Princeton, NJ (1996)
21. Kaschiev, D.: Nucleation: Basic Theory with Applications. Butterworth-Heinemann, Oxford (2000)
22. Price, S.L.: Computed crystal energy landscapes for understanding and predicting organic crystal structures and polymorphism. Acc. Chem. Res. **42**, 117–126 (2008)
23. Erdemir, D., Lee, A.Y., Myerson, A.S.: Nucleation of crystals from solution: classical and two-step models. Acc. Chem. Res. **42**, 621–629 (2009)
24. Vekilov, P.G.: Nucleation. Cryst. Growth Des. **10**, 5007–5019 (2010)
25. Auer, S., Frenkel, D.: Quantitative prediction of crystal-nucleation rates for spherical colloids: a computational approach. Annu. Rev. Phys. Chem. **55**, 333–361 (2004)
26. Anwar, J., Zahn, D.: Uncovering molecular processes in crystal nucleation and growth by using molecular simulation. Angewandte Chemie-International Edition **50**, 1996–2013 (2011)
27. Palmer, J.C., Debenedetti, P.G.: Recent advances in molecular simulation: a chemical engineering perspective. AIChE J. **61**, 370–383 (2015)
28. TenWolde, P.R., RuizMontero, M.J., Frenkel, D.: Numerical calculation of the rate of crystal nucleation in a Lennard-Jones system at moderate undercooling. J. Chem. Phys. **104**, 9932–9947 (1996)

29. Vehkamäki, H., Ford, I.J.: Critical cluster size and droplet nucleation rate from growth and decay simulations of Lennard-Jones clusters. J. Chem. Phys. **112**, 4193–4202 (2000)
30. Auer, S., Frenkel, D.: Prediction of absolute crystal-nucleation rate in hard-sphere colloids. Nature **409**, 1020–1023 (2001)
31. Moroni, D., ten Wolde, P.R., Bolhuis, P.G.: Interplay between structure and size in a critical crystal nucleus. Phys. Rev. Lett. **94**, 235703 (2005)
32. Trudu, F., Donadio, D., Parrinello, M.: Freezing of a Lennard-Jones fluid: from nucleation to spinodal regime. Phys. Rev. Lett. **97**, 105701 (2006)
33. Desgranges, C., Delhommelle, J.: Insights into the molecular mechanism underlying polymorph selection. J. Am. Chem. Soc. **128**, 15104–15105 (2006)
34. Desgranges, C., Delhommelle, J.: Polymorph selection during the crystallization of Yukawa systems. J. Chem. Phys. **126**, 054501 (2007)
35. Jungblut, S., Dellago, C.: Heterogeneous crystallization on tiny clusters. EPL (Europhysics Letters) **96**, 56006 (2011)
36. Beckham, G.T., Peters, B.: Optimizing nucleus size metrics for liquid-solid nucleation from transition paths of near-nanosecond duration. J. Phys. Chem. Lett. **2**, 1133–1138 (2011)
37. Chkonia, G., Wölk, J., Strey, R., Wedekind, J., Reguera, D.: Evaluating nucleation rates in direct simulations. J. Chem. Phys. **130**, 064505 (2009)
38. Radhakrishnan, R., Trout, B.L.: Nucleation of hexagonal ice (Ih) in liquid water. J. Am. Chem. Soc. **125**, 7743–7747 (2003)
39. Li, T., Donadio, D., Russo, G., Galli, G.: Homogeneous ice nucleation from supercooled water. Phys. Chem. Chem. Phys. **13**, 19807–19813 (2011)
40. Reinhardt, A., Doye, J.P.K.: Free energy landscapes for homogeneous nucleation of ice for a monatomic water model. J. Chem. Phys. **136**, 054501 (2012)
41. Sanz, E., Vega, C., Espinosa, J.R., Caballero-Bernal, R., Abascal, J.L.F., Valeriani, C.: Homogeneous ice nucleation at moderate supercooling from molecular simulation. J. Am. Chem. Soc. **135**, 15008–15017 (2013)
42. Sear, R.P.: The non-classical nucleation of crystals: microscopic mechanisms and applications to molecular crystals, ice and calcium carbonate. Int. Mater. Rev. **57**, 328–356 (2012)
43. Andrey, V.B., Jamshed, A., Ruslan, D., Richard, H.: Challenges in molecular simulation of homogeneous ice nucleation. J. Phys.: Condens. Matter **20**, 494243 (2008)
44. Reinhardt, A., Doye, J.P.K.: Note: homogeneous TIP4P/2005 ice nucleation at low supercooling. J. Chem. Phys. **139**, 096102 (2013)
45. Joswiak, M.N., Duff, N., Doherty, M.F., Peters, B.: Size-dependent surface free energy and tolman-corrected droplet nucleation of TIP4P/2005 water. J. Phys. Chem. Lett. **4**, 4267–4272 (2013)
46. Holten, V., Limmer, D.T., Molinero, V., Anisimov, M.A.: Nature of the anomalies in the supercooled liquid state of the mW model of water. J. Chem. Phys. **138**, 174501 (2013)
47. Valeriani, C., Sanz, E., Frenkel, D.: Rate of homogeneous crystal nucleation in molten NaCl. J. Chem. Phys. **122** (2005)
48. Quigley, D., Rodger, P.M.: Free energy and structure of calcium carbonate nanoparticles during early stages of crystallization. J. Chem. Phys. **128**, 221101 (2008)
49. Li, T., Donadio, D., Galli, G.: Nucleation of tetrahedral solids: a molecular dynamics study of supercooled liquid silicon. J. Chem. Phys. **131**, 224519 (2009)
50. Yi, P., Rutledge, G.C.: Molecular simulation of crystal nucleation in n-octane melts. J. Chem. Phys. **131**, 134902 (2009)
51. Saika-Voivod, I., Poole, P.H., Bowles, R.K.: Test of classical nucleation theory on deeply supercooled high-pressure simulated silica. J. Chem. Phys. **124**, 224709 (2006)
52. Agarwal, V., Peters, B.: Nucleation near the eutectic point in a Potts-lattice gas model. J. Chem. Phys. **140**, 084111 (2014)
53. Singh, M., Dhabal, D., Nguyen, A.H., Molinero, V., Chakravarty, C.: Triplet correlations dominate the transition from simple to tetrahedral liquids. Phys. Rev. Lett. **112**, 147801 (2014)
54. Shah, M., Santiso, E.E., Trout, B.L.: Computer simulations of homogeneous nucleation of benzene from the melt. J. Phys. Chem. B **115**, 10400–10412 (2011)

55. Giberti, F., Salvalaglio, M., Mazzotti, M., Parrinello, M.: Insight into the nucleation of urea crystals from the melt. Chem. Eng. Sci. **121**, 51–59 (2015)
56. Yu, T.-Q., Chen, P.-Y., Chen, M., Samanta, A., Vanden-Eijnden, E., Tuckerman, M.: Order-parameter-aided temperature-accelerated sampling for the exploration of crystal polymorphism and solid-liquid phase transitions. J. Chem. Phys. **140**, 214109 (2014)
57. Samanta, A., Tuckerman, M.E., Yu, T.-Q.: E, W. Microscopic mechanisms of equilibrium melting of a solid. Science **346**, 729–732 (2014)
58. Pedersen, U.R., Hummel, F., Dellago, C.: Computing the crystal growth rate by the interface pinning method. J. Chem. Phys. **142**, 044104 (2015)
59. Maragliano, L., Fischer, A., Vanden-Eijnden, E., Ciccotti, G.: String method in collective variables: minimum free energy paths and isocommittor surfaces. J. Chem. Phys. **125**, 024106 (2006)
60. Vanden-Eijnden, E., Venturoli, M.: Revisiting the finite temperature string method for the calculation of reaction tubes and free energies. J. Chem. Phys. **130**, 194103 (2009)
61. Maragliano, L., Vanden-Eijnden, E., Roux, B.: Free energy and kinetics of conformational transitions from voronoi tessellated milestoning with restraining potentials. J. Chem. Theory Comput. **5**, 2589–2594 (2009)
62. Vanden-Eijnden, E., Venturoli, M.: Markovian milestoning with Voronoi tessellations. J. Chem. Phys. **130**, 194101 (2009)
63. Ovchinnikov, V., Karplus, M., Vanden-Eijnden, E.: Free energy of conformational transition paths in biomolecules: the string method and its application to myosin VI. J. Chem. Phys. **134**, 085103 (2011)
64. Miller, T.F., III; Vanden-Eijnden, E., Chandler, D.: Solvent coarse-graining and the string method applied to the hydrophobic collapse of a hydrated chain. In: Proceedings of the National Academy of Sciences of the United States of America, vol. 104, pp. 14559–14564 (2007)
65. Santiso, E.E., Trout, B.L.: A general set of order parameters for molecular crystals. J. Chem. Phys. **134**, 064109 (2011)
66. Santiso, E.E., Trout, B.L.: A general method for molecular modeling of nucleation from the melt. J. Chem. Phys. **143**, 174109 (2015)
67. He, X., Shen, Y., Hung, F.R., Santiso, E.E.: Molecular simulation of homogeneous nucleation of crystals of an ionic liquid from the melt. J. Chem. Phys. **143**, 124506 (2015)
68. Barducci, A., Bonomi, M., Parrinello, M.: Metadynamics. Wiley Interdis. Rev. Comput. Mol. Sci. **1**, 826–843 (2011)
69. Allen, F.H.: The Cambridge structural database: a quarter of a million crystal structures and rising. Acta Crystallographica Sect. B-Struct. Sci. **58**, 380–388 (2002)
70. Arduengo, A.J., Dias, H.V.R., Harlow, R.L., Kline, M.: Electronic stabilization of nucleophilic carbenes. J. Am. Chem. Soc. **114**, 5530–5534 (1992)
71. Lopes, J.N.C., Deschamps, J., Padua, A.A.H.: Modeling ionic liquids using a systematic all-atom force field. J. Phys. Chem. B **108**, 2038–2047 (2004)
72. Canongia Lopes, J.N., Padua, A.A.H.: Molecular force field for ionic liquids III: Imidazolium, pyridinium, and phosphonium cations; chloride, bromide, and dicyanamide anions. J. Phys. Chem. B **110**, 19586–19592 (2006)
73. Lopes, J.N.C., Padua, A.A.H.: Molecular force field for ionic liquids composed of triflate or bistriflylimide anions. J. Phys. Chem. B **108**, 16893–16898 (2004)
74. Shimizu, K., Almantariotis, D., Gomes, M.F.C., Padua, A.A.H., Lopes, J.N.C.: Molecular force field for ionic liquids V: hydroxyethylimidazolium, dimethoxy-2-methylimidazolium, and fluoroalkylimidazolium cations and bis(fluorosulfonyl)amide, perfluoroalkanesulfonylamide, and fluoroalkylfluorophosphate anions. J. Phys. Chem. B **114**, 3592–3600 (2010)
75. Lopes, J.N.C., Padua, A.A.H., Shimizu, K.: Molecular force field for ionic liquids IV: trialkylimidazolium and alkoxycarbonyl-imidazolium cations; alkylsulfonate and alkylsulfate anions. J. Phys. Chem. B **112**, 5039–5046 (2008)

76. Fannin, A.A., Floreani, D.A., King, L.A., Landers, J.S., Piersma, B.J., Stech, D.J., Vaughn, R. L., Wilkes, J.S., Williams, J.L.: Properties of 1,3-dialkylimidazolium chloride aluminum-chloride ionic liquids. 2. phase-transitions, densities, electrical conductivities, and viscosities. J. Phys. Chem. **88**, 2614–2621 (1984)
77. Phillips, J.C., Braun, R., Wang, W., Gumbart, J., Tajkhorshid, E., Villa, E., Chipot, C., Skeel, R.D., Kale, L., Schulten, K.: Scalable molecular dynamics with NAMD. J. Comput. Chem. **26**, 1781–1802 (2005)
78. Darden, T., York, D., Pedersen, L.: Particle mesh ewald—an n.log(n) method for ewald sums in large systems. J. Chem. Phys. **98**, 10089–10092 (1993)
79. Hess, B., Bekker, H., Berendsen, H.J.C., Fraaije, J.: LINCS: A linear constraint solver for molecular simulations. J. Comput. Chem. **18**, 1463–1472 (1997)
80. Vanden-Eijnden, E.: Some recent techniques for free energy calculations. J. Comput. Chem. **30**, 1737–1747 (2009)
81. Pruppacher, H.R.: A new look at homogeneous ice nucleation in supercooled water drops. J. Atmos. Sci. **52**, 1924–1933 (1995)
82. Taborek, P.: Nucleation in emulsified supercooled water. Phys. Rev. B **32**, 5902–5906 (1985)